electronics

MDPI

Article

Dead-Time Correction Applied for Extended Flux-Based Sensorless Control of Assisted PMSMs in Electric Vehicles

Cheng Lin [1,2,*], Jilei Xing [2] and Xingming Zhuang [3]

[1] Collaborative Innovation Center of Electric Vehicles in Beijing, Beijing Institute of Technology, Beijing 100081, China
[2] National Engineering Laboratory for Electric Vehicles, Beijing Institute of Technology, Beijing 100081, China; xingjilei699@163.com
[3] BIT HuaChuang Electirc Vehicle Technology Co., Ltd., Beijing 100081, China; zhuangxingming@huachuangev.com
* Correspondence: lincheng@bit.edu.cn

Abstract: Sensorless control technology of PMSMs is of great importance for safety and reliability in electric vehicles. Among all existing methods, only the extended flux-based method has great performance over all speed range. However, the accuracy and reliability of the extended flux rotor position observer are greatly affected by the dead-time effect. In this paper, the extended flux-based observer is adopted to develop a sensorless control system. The influence of dead-time effect on the observer is analyzed and a dead-time correction method is specially designed to guarantee the reliability of the whole control system. A comparison of estimation precision among the extended flux-based method, the electromotive force (EMF)-based method and the high frequency signal injection method is given by simulations. The performance of the proposed sensorless control system is verified by experiments. The experimental results show that the proposed extended flux-based sensorless control system with dead-time correction has satisfactory performance over full speed range in both loaded and non-loaded situations. The estimation error of rotor speed is within 4% in all working conditions. The dead-time correction method improves the reliability of the control system effectively.

Keywords: permanent magnet synchronous motor; sensorless control; extended flux; electric vehicle; dead-time correction

Citation: Lin, C.; Xing, J.; Zhuang, X. Dead-Time Correction Applied for Extended Flux-Based Sensorless Control of Assisted PMSMs in Electric Vehicles. *Electronics* **2021**, *10*, 220. https://doi.org/10.3390/electronics10020220

Received: 2 December 2020
Accepted: 18 January 2021
Published: 19 January 2021

1. Introduction

Permanent magnet synchronous motors (PMSMs) have been extensively adopted in electric vehicles in recent years due to positive features such as high-power density and high efficiency [1]. They are not only used as traction motors but also used as assisted motors in steering system and braking system, especially in electric commercial vehicles [2]. For the applications except for traction motors, the position sensors of PMSMs are eliminated in consideration of cost and mounting space [3]. Moreover, sensorless control technology is also used for fault detection and fault tolerant control of the traction motors in case of failures of position sensors [4].

Existing sensorless control technology can be classified into two categories: signal injection methods and model-based observer methods [5,6]. Signal injection methods can give precise rotor position estimation by analyzing current response to specific high-frequency voltage pulses. However, these methods can only perform well at standstill and low speeds [7,8]. Model-based observer methods can be further divided into the EMF-based methods and the extended flux-based methods [9]. The EMF-based methods are the most widely used methods for rotor position estimation [10–12]. However, their performance deteriorates drastically at low speeds because the EMF is too low to be detected [13]. As for the extended flux-based methods, they can detect the rotor position information under full speed range, because the extended flux is always detectable at any speed [14].

Studies about the extended flux-based methods are relatively rare compared to other sensorless control technology, as there are many problems in practical application. For example, the initial rotor position and the permanent magnet flux linkage must be accurate when using the extended flux-based methods [15]. Besides these, the effect of dead time must be taken into consideration when the motor operates at low speed [16]. In most proposals related to the extended flux-based methods, conventional dead-time compensation is applied in the control system without delving into details [17,18]. In some other studies of sensorless control system, the dead-time compensation is executed with the help of the estimated rotor position [19]. However, these simple compensation methods are not accurate and even not reliable due to variation of dead-time compensation time and current clamping effects. Advanced dead-time compensation methods based on observers of dead-time compensation time are proposed in recent years to realize adaptive dead-time compensation [20,21]. Some self-commissioning methods considering multiple nonlinear factors, such as the effect of parasitic capacitors, are studied to make the compensation more accurate [22,23]. All these advanced methods have shown great characteristics in applications of traction motor control system, with the help of precise current sampling by Hall elements. As for the applications in assisted motors, current sampling is realized by sampling resistance, the precision of which deteriorates under small current conditions. Under this circumstance, dead-time compensation may be inaccurate and bring negative impact to the reliability of the control system. Consequently, application of dead-time compensation is uncommon in sensorless control system of assisted motors. In this paper, a simpler way to deal with this problem is provided by specially designing a dead-time corrector for the extended flux-based method and limiting the impact of dead-time correction to the position estimator.

The paper is organized as follows. The theory of the extended flux-based sensorless control technology is introduced in Section 2. Then, the dead-time correction method is designed in Section 3. The performance of the proposed sensorless control system is verified by experimental results in Section 4. Finally, the key features of the proposed sensorless control system are summarized in Section 5.

2. Extended Flux-Based Sensorless Control Technology

2.1. Mathematical Model of PMSM

The model of PMSM in the rotating reference frame can be written as follows [24]:

$$\begin{cases} u_d = R_s i_d + L_d \frac{di_d}{dt} - \omega_e \lambda_q \\ u_q = R_s i_q + L_q \frac{di_q}{dt} + \omega_e \lambda_d \end{cases} \tag{1}$$

where u_d, u_q, i_d, i_q, L_d, L_q, λ_d and λ_q are the stator voltage components, stator current components, inductances and flux linkage along the direct axis (d-axis) and the quadrature axis (q-axis), ω_e is electrical speed of the motor and R_s is the phase winding resistance. The stator flux linkages can be expressed as:

$$\begin{cases} \lambda_d = L_d i_d \lambda_f \\ \lambda_q = L_q i_q \end{cases} \tag{2}$$

where λ_f is the permanent magnet flux linkage of the motor. In (2), the stator flux linkages are calculated with the stator current, which is called current model for simplicity in this paper.

In order to simplify the model of PMSM in the stationary reference frame, the concept of extended flux is developed and defined as:

$$\lambda_{ext} = \lambda_f - (L_q - L_d) i_d \tag{3}$$

By combining (3) and (1), the model of PMSM can be rewritten as:

$$\begin{cases} u_d = R_s i_d + L_q \frac{di_d}{dt} - \omega_e L_q i_q + \frac{d\lambda_{ext}}{dt} \\ u_q = R_s i_q + L_q \frac{di_q}{dt} + \omega_e L_q i_d + \omega_e \lambda_{ext} \end{cases} \tag{4}$$

Furthermore, the extended flux in the stationary reference frame is defined as:

$$\begin{cases} \lambda_{ext,\alpha} = \lambda_{ext} \cos\theta_e \\ \lambda_{ext,\beta} = \lambda_{ext} \sin\theta_e \end{cases} \tag{5}$$

where θ_e is the rotor position of the motor. Then (2) can be converted into the stationary reference frame with the help of the extended flux, as shown in (6).

$$\begin{cases} \lambda_\alpha = L_q i_\alpha + \lambda_{ext,\alpha} \\ \lambda_\beta = L_q i_\beta + \lambda_{ext,\beta} \end{cases} \tag{6}$$

where i_α, i_β, λ_α and λ_β are the stator current components and flux linkage in the two-phase stationary reference frame. It is obvious that the extended flux in the stationary frame contains the information of rotor position. The extended flux can be derived not only by the current model, but also by the voltage model in (7) which can be deduced from (4) and (6).

$$\begin{cases} \frac{d\lambda_\alpha}{dt} = u_\alpha - R_s i_\alpha \\ \frac{d\lambda_\beta}{dt} = u_\beta - R_s i_\beta \end{cases} \tag{7}$$

where u_α and u_β are the stator voltage components in the two-phase stationary reference frame.

An illustration diagram of the equations above is summarized in Figure 1, including the voltage model and current model used in the extended flux-based sensorless control technology. T_{park} in the diagram is the Park transformation matrix.

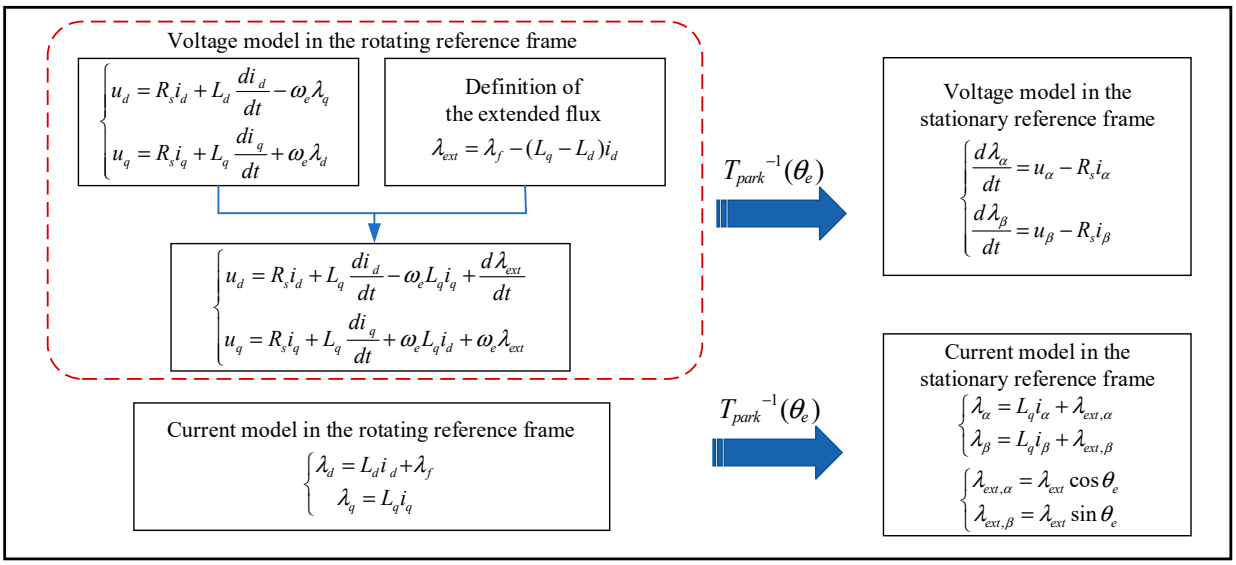

Figure 1. Illustration diagram of the model equations used in the extended flux-based sensorless control technology.

2.2. Rotor Position Estimation-Based on Extended Flux Observer

The voltage model in (7) can be used as an open-loop flux observer [25]. However, the estimation error caused by some practical issues, e.g., the DC offset of current sensors will be accumulated by the integrator [26]. Another flux observer is constructed by applying the voltage model and the current model in the meantime. The estimation error between the two models is used as the input of a PI compensator, the output of which is used to correct

the voltage model. The structure of this closed-loop flux observer is shown in Figure 2. The observer can be expressed as follows:

$$\begin{cases} \frac{d\hat{\lambda}_{\alpha,u}}{dt} = u_\alpha - R_s i_\alpha + u_{comp,\alpha} \\ \frac{d\hat{\lambda}_{\beta,u}}{dt} = u_\beta - R_s i_\beta + u_{comp,\beta} \end{cases} \tag{8}$$

$$\begin{cases} \hat{\lambda}_{d,i} = L_d \hat{i}_d + \lambda_f \\ \hat{\lambda}_{q,i} = L_q \hat{i}_q \\ \hat{\lambda}_{\alpha\beta,i} = {T_{park}}^{-1}(\hat{\theta}_e)\hat{\lambda}_{dq,i} \end{cases} \tag{9}$$

where $\hat{\lambda}_{\alpha,u}$ and $\hat{\lambda}_{\beta,u}$ are the estimated quantities of λ_α and λ_β using the voltage model, $u_{comp,\alpha}$ and $u_{comp,\beta}$ are the output of the PI compensator, $\hat{\lambda}_{d,i}$ and $\hat{\lambda}_{q,i}$ are the estimated quantities of λ_d and λ_q using the current model, $\hat{\lambda}_{\alpha\beta,i}$ is the estimated quantity of λ_α and λ_β using the current model, $\hat{\theta}_e$ is the estimated quantity of θ_e and T_{park} is the Park transformation matrix. The compensating voltage can be calculated by the PI compensator:

$$\begin{cases} u_{comp,\alpha} = (K_p + \frac{K_i}{s})(\hat{\lambda}_{\alpha,i} - \hat{\lambda}_{\alpha,u}) \\ u_{comp,\beta} = \left(K_p + \frac{K_i}{s}\right)(\hat{\lambda}_{\beta,i} - \hat{\lambda}_{\beta,u}) \end{cases} \tag{10}$$

where K_p and K_i are the gains of the PI compensator.

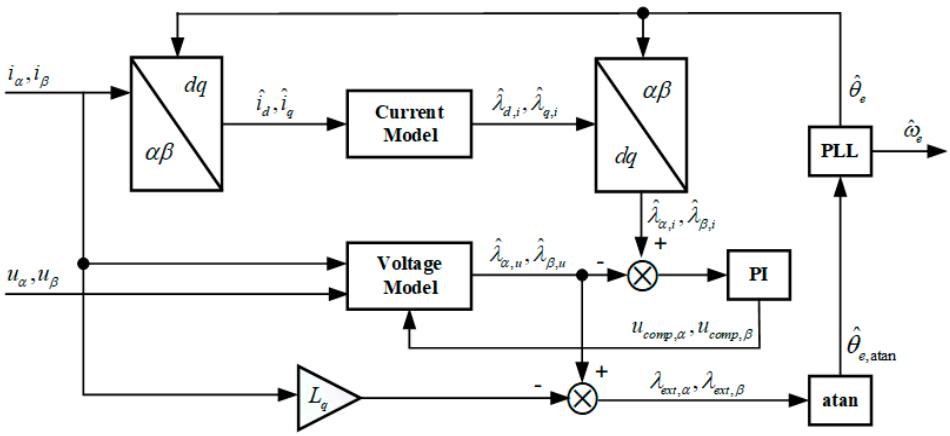

Figure 2. Structure of the extended flux-based rotor position observer.

With the help of the PI compensator, the accumulated error can be eliminated. Furthermore, the estimated rotor speed is absent in the observer, which excludes the bad effect of inaccurate speed estimation. The stability of the observer is analyzed and demonstrated in [27]. Once the estimated stator flux is obtained, the extended flux and the rotor position can be deduced as:

$$\begin{cases} \hat{\lambda}_{ext,\alpha} = \hat{\lambda}_{\alpha,u} - L_q i_\alpha \\ \hat{\lambda}_{ext,\beta} = \hat{\lambda}_{\beta,u} - L_q i_\beta \\ \hat{\theta}_{e,\text{atan}} = \arctan(\hat{\lambda}_{ext,\beta}/\hat{\lambda}_{ext,\alpha}) \end{cases} \tag{11}$$

where $\hat{\theta}_{e,\text{atan}}$ is the estimated rotor position using the arctangent function. Then a phase-locked loop (PLL) observer is used to extract the rotor position and speed information in consideration of noises and harmonic components within the observed signals [28]. The structure of the PLL observer is shown in Figure 3 and the closed-loop transfer function of the PLL can be derived as:

$$G_{PLL} = \frac{K_{p,PLL}s + K_{i,PLL}}{s^2 + K_{p,PLL}s + K_{i,PLL}} \tag{12}$$

where $K_{p,PLL}$ and $K_{i,PLL}$ are the gains of the phase-locked loop (PLL) observer.

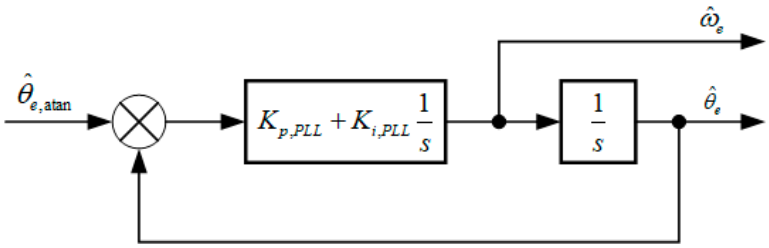

Figure 3. Structure of the PLL observer.

Both the advantages of the current model at low speed and that of the voltage model at high speed are taken in the position estimation method above, making it a full-speed-range sensorless control technology. This feature is of great importance for fault-tolerant control of traction motors, because the operating speed of traction motors changes rapidly, and frequent technology switching between high and low speed will lead to unreliability of the whole system. The comparison between the extended flux-based estimation method and the other two mainstream methods, i.e., the high frequency signal injection method and the EMF-based method is given in Figure 4. The motor is started from standstill and accelerated to 1500 rpm (rated speed of the tested motor) with speed sensor under rated load. The three estimation methods are applied at the same time. The simulation results validate that only the extended flux-based method can realize accurate estimation in full speed range. In Figure 5, the estimation results of the extended flux-based method are used to realize sensorless control of the motor, which show its accuracy and reliability.

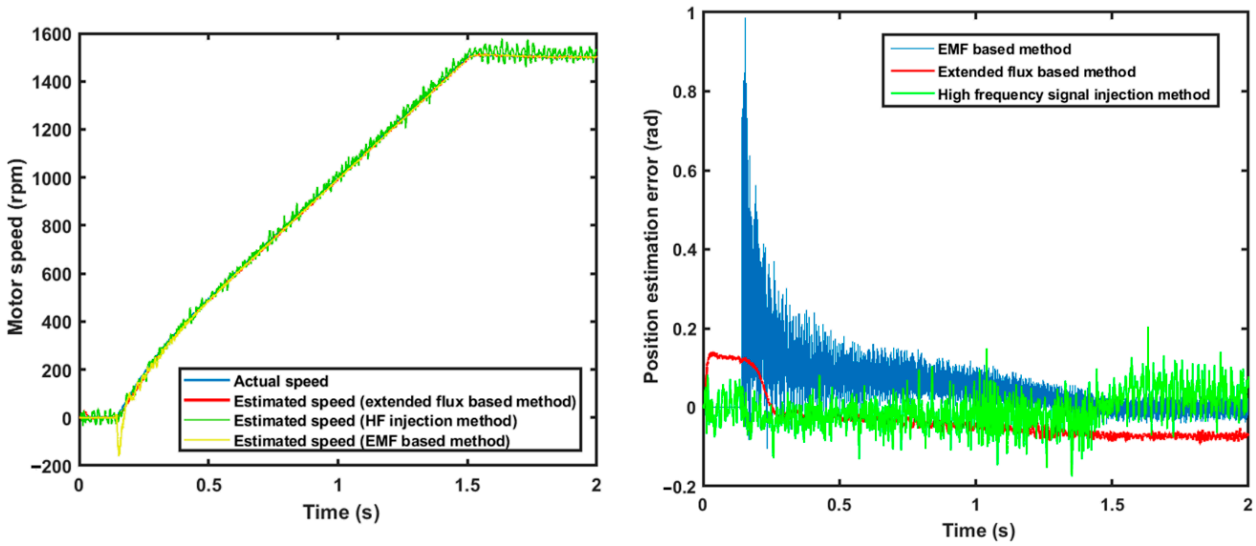

(**a**) (**b**)

Figure 4. Comparison of the three mainstream rotor position estimation methods: (**a**) Speed estimation results over full speed range; (**b**) Rotor position estimation error over full speed range.

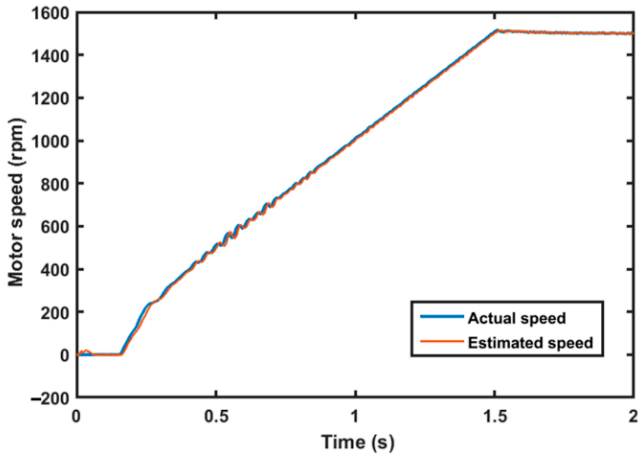

Figure 5. Motor speed during the startup process using the extended flux-based observer.

3. Dead-Time Correction for Sensorless Control System

3.1. Dead-Time Effect

As the switching feature of insulated gate bipolar transistors (IGBTs) is not ideal, the two IGBTs in an inverter leg must be in an off state in the meantime for a time during every switching period, which is called the dead time [29]. Affected by the dead time, there is a deviation between the reference stator voltage and the actual stator voltage. This deviation can be expressed as function of dead time, switching period, DC-link voltage and the direction of stator current.

$$\Delta u_x = \frac{U_{dc} t_d}{T_s} \cdot sign(i_x) \tag{13}$$

where U_{dc} is the DC-link voltage, t_d is the dead time and T_s is the switching period. The dead time is composed of controlled dead-time t_{cd}, turn-on time t_{on}, turn-off time t_{off}, and average on time $t_{a,on}$ [26], which can be expressed as:

$$t_d = t_{cd} + t_{on} - t_{off} + t_{a,on} = t_{cd} + t_{on} - t_{off} + \frac{U_{on}}{U_{dc}} T_s \tag{14}$$

where U_{on} is the average on voltage, which is defined as:

$$U_{on} = \begin{cases} \frac{T_{on}}{T_s} U_s + \frac{T_{off}}{T_s} U_d, i > 0 \\ \frac{T_{off}}{T_s} U_s + \frac{T_{on}}{T_s} U_d, i < 0 \end{cases} \tag{15}$$

where U_s and U_d are on-voltage drops of switching devices and diodes, and T_{on}, T_{off} are on-period and off-period of the upper-arm of inverter leg.

For most applications, the stator voltage used in the flux observer above is the reference voltage rather than the actual one. The voltage deviation will produce additional error for rotor position estimation. Generally, the deviation voltage is about 1~5% of the DC-link voltage. When the reference voltage is high enough, estimation error caused by the dead-time effect is negligible. However, the stator voltage will become quite low at low speed. When the extended flux-based method is executed at low speed, the voltage deviation may become equal to the reference voltage, which will cause huge estimation error and out-of-control failure. Simulation results in Figure 6 show the position estimation error of the observer based on extended flux during the startup process with different dead time. Operating status of the motor is the same as that in Figure 3. Large estimation error can be observed at low speed and becomes much bigger as the dead time increases.

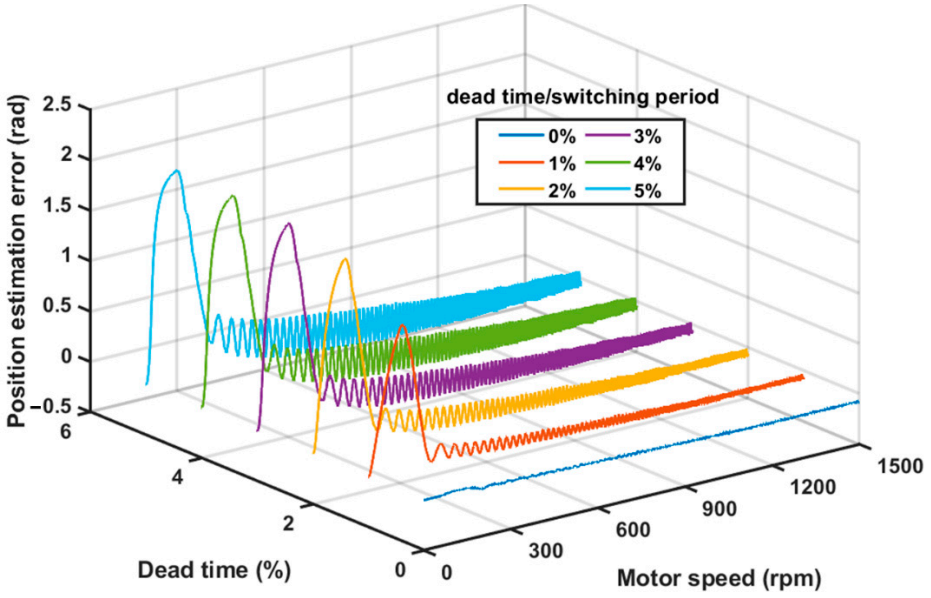

Figure 6. Rotor position estimation error of the extended flux-based observer with different dead time.

3.2. Dead-Time Correction Method

The common solution for dead-time effect is the dead-time compensation technology. The deviation of stator voltage in stationary reference frame is calculated according to (13) and added to the reference voltage. The dead-time compensation methods perform effectively in applications of traction motors, because the current sampling is precise with Hall elements. However, in consideration of cost, phase current is inspected by setting sampling resistances in series in the three-phase circuit in applications of assisted motors. Though the power dissipation of the sampling resistance is negligibly small, the sampling precision deteriorates under small current conditions. Consequently, dead-time compensation may be unreasonable and bring negative impact on stability of the vector control system.

Instead of compensating the output voltage, correcting the stator voltage used in the extended flux observer will be an effective and simple solution for this problem. By limiting the impact of dead-time correction to the rotor position estimator, reliability of the vector control system can be guaranteed. The structure of the extended flux-based sensorless control system with dead-time correction is shown in Figure 7. The stator voltage is used only in the voltage-model-based observer in (8), which is corrected by the dead-time voltage deviation as follows:

$$\begin{cases} u_\alpha^* = u_\alpha - \Delta u_\alpha \\ u_\beta^* = u_\beta - \Delta u_\beta \end{cases} \tag{16}$$

The voltage deviation in the stationary reference frame can be calculated by (13) without the rotor position information.

$$\begin{bmatrix} \Delta u_\alpha \\ \Delta u_\beta \end{bmatrix} = \frac{2}{3} \begin{bmatrix} 1 & -1/2 & -1/2 \\ 0 & \sqrt{3}/2 & \sqrt{3}/2 \end{bmatrix} \begin{bmatrix} \Delta u_a \\ \Delta u_b \\ \Delta u_c \end{bmatrix} \tag{17}$$

Then the voltage-model-based observer in (8) can be rewritten as:

$$\begin{cases} \frac{d\hat{\lambda}_{\alpha,u}}{dt} = u_\alpha^* - R_s i_\alpha + u_{comp,\alpha} \\ \frac{d\hat{\lambda}_{\beta,u}}{dt} = u_\beta^* - R_s i_\beta + u_{comp,\beta} \end{cases} \tag{18}$$

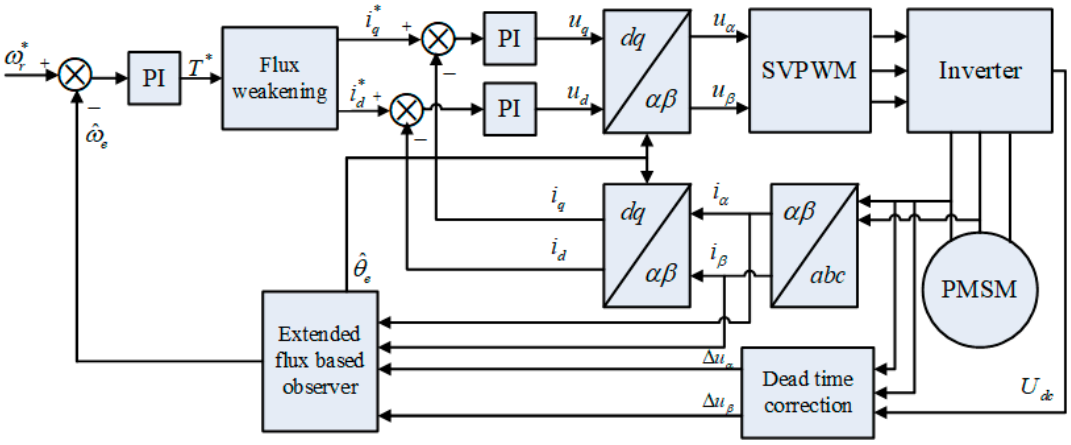

Figure 7. Structure of the extended flux-based sensorless control system with dead-time correction.

The proposed dead-time correction method is devoted to extended flux-based sensorless control system, because the dead-time effect has less effect on the estimation precision of signal injection methods. Applications of the EMF-based methods demand high-precision dead-time compensation at low speeds. The dead-time correction is applied to the extended flux observer rather than the vector control system to avoid adverse effect of inaccurate dead-time compensation for the whole control system. Thanks to the current model and PLL observer, impact of less accurate dead-time calculation is tolerant for the extended flux observer. Furthermore, it is much simpler than real-time dead-time compensation, which can show better performance only with accurate rotor position information. Based on the analysis above, the proposed extended flux-based sensorless control system with dead-time correction is more suitable for applications in assisted motor. It can also be used for the traction motors with the consideration of its simplicity. The structure of the extended flux-based sensorless control system with dead-time correction is shown in Figure 7.

4. Experimental Results

The purpose of this section is to verify the properties of the proposed extended flux-based sensorless control system with dead-time correction. For the experiments, a homemade three-phase two-level IGBT inverter switching at 6 kHz and a DC voltage source of 540 V are applied. The strategy is realized with a digital controller based on DSP TMS320F28035 with a clock speed of 60 MHz [30]. The motor is loaded by a hydraulic circuit, which consists of a hydraulic oil pump, a hydraulic valve, an oil reservoir and high-pressure oil pipes. Furthermore, an optical encoder is installed between the tested PMSM and the pump to validate the motor speed and position estimation. The experimental setup is shown in Figure 8. The parameters of the tested PMSM are given in Table 1.

Table 1. Motor parameters.

Denotation	Symbol	Value
Rated power (kW)	P_R	3
Rated current (A)	I_R	10
Rated speed (rpm)	n_R	1500
Rated load (N·m)	T_R	23
Rated frequency (Hz)	f_R	100
Number of pole pairs	n_p	4
Stator resistance (Ω)	R_s	1.08
d-axis inductance (mH)	L_d	12.52
q-axis inductance (mH)	L_q	23.37
Flux linkage (Wb)	λ_f	0.26

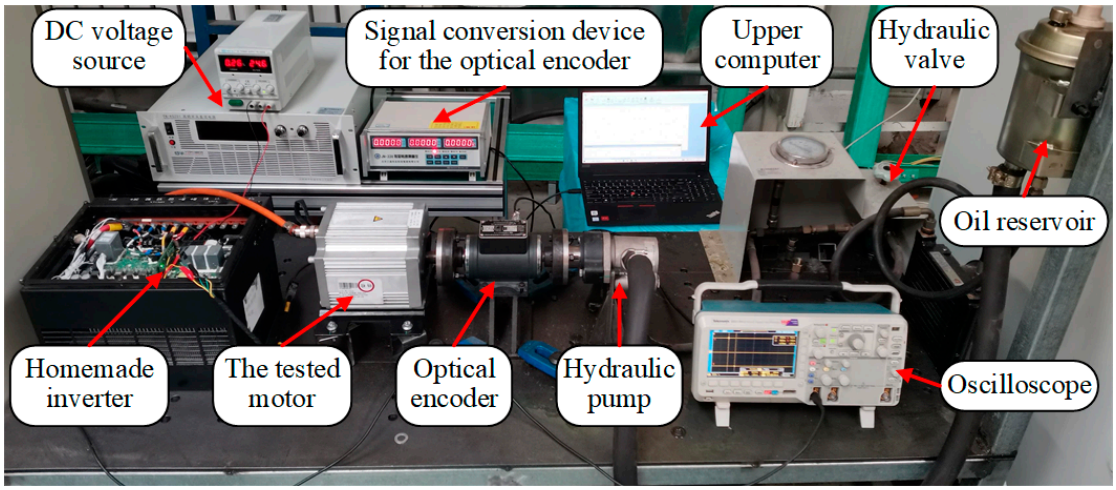

Figure 8. Experimental setup.

The motor is started from standstill and accelerated to its rated speed in the experiment. The hydraulic valve is used to tune the load. The performance of the sensorless control system proposed in this paper is first demonstrated under no load. Then the motor is started under rated load to verify its operating performance under load.

Experimental verification under no load is conducted firstly and the results are shown in Figure 9a. It can be seen that the proposed extended flux-based sensorless control system shows great performance over full speed range. No large speed or torque ripples can be found during the whole process. The speed estimation error is within 55 rpm. The same experiment is conducted under rated load, where the oil pressure reaches 11 MPa. Experimental results in Figure 9b show that the proposed method performs well with higher output torque. The speed estimation error is within 57 rpm over full speed range. It can be seen that the performance under low speeds is poorer than that at high speeds due to less accurate dead-time correction. However, assisted motors of electric vehicles hardly work under low speeds. Reliable start-up process from standstill to rated speed is needed and can be guaranteed by the dead-time correction method.

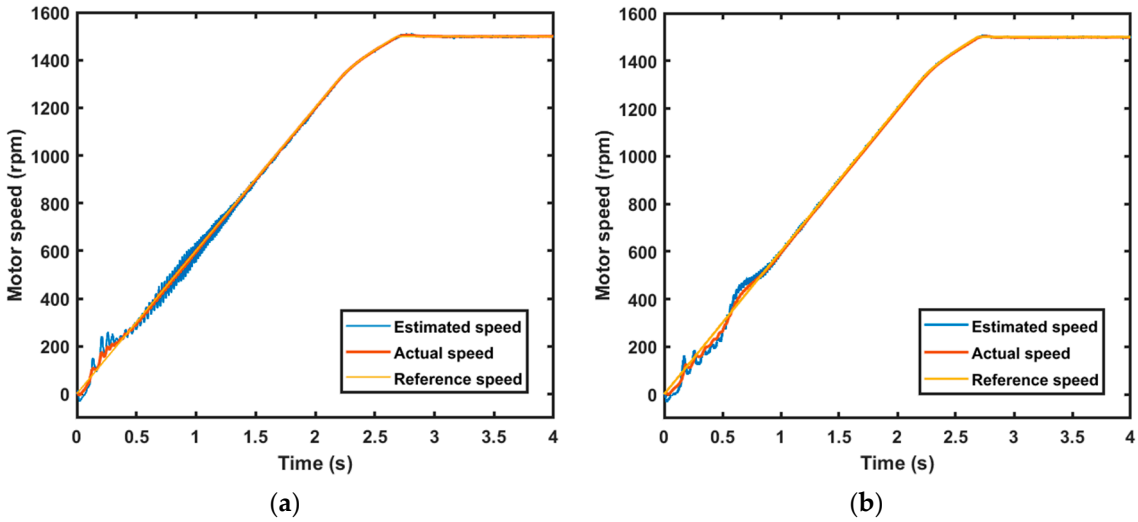

Figure 9. Motor speed during the startup process: (**a**) Non-loaded situations; (**b**) Loaded situations.

To validate the influence of dead-time correction, the experiment under rated load is repeated with 50% dead-time correction and no dead-time correction respectively. As the motor cannot be started without dead-time correction under load, the experiment is executed under no load. Transients of the a-phase current at the startup moment are given

in Figure 10. It can be found that the a-phase current with full dead-time correct is the smoothest one, indicating the most accurate rotor position estimation. The peak value of a-phase current without dead-time correction is two times of that with dead-time correction.

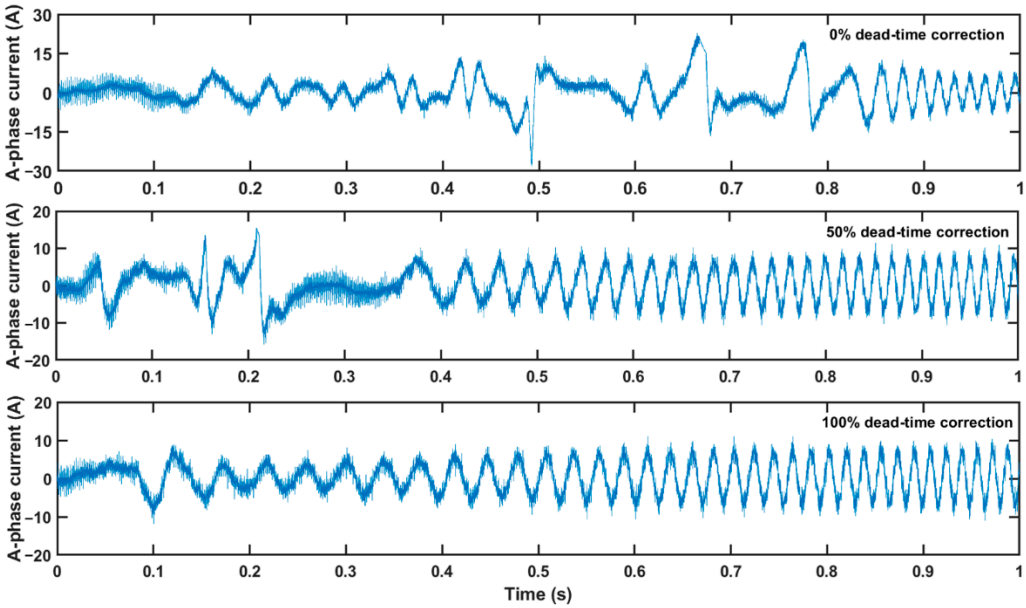

Figure 10. A-phase current with different dead-time correction.

From the experimental results above, it can be observed that the proposed extended flux-based sensorless control system has satisfactory performance over full speed range in both loaded and non-loaded situations. The dead-time correction is essential for the reliability of the control system.

5. Conclusions

An extended flux-based sensorless control system with dead-time correction is proposed in this paper to achieve reliable control of PMSMs with only one rotor position estimation method over full speed range. To guarantee the reliability of the whole control system, a dead-time correction method devoted to the extended flux observer is designed. The performance of the proposed sensorless control system was verified by experimental results. The proposed extended flux-based sensorless control system with dead-time correction best suits the applications in assisted motors of electrical vehicles and can also be used for fault detection and fault tolerant control of the traction motors of electric vehicles.

Author Contributions: Conceptualization, C.L. and J.X.; methodology, J.X.; software, J.X.; validation, J.X.; formal analysis, J.X.; investigation, X.Z.; resources, C.L.; data curation, J.X.; writing—original draft preparation, J.X.; writing—review and editing, X.Z.; visualization, J.X.; supervision, X.Z.; project administration, C.L.; funding acquisition, C.L. All authors have read and agreed to the published version of the manuscript.

Funding: This research was funded by the National Natural Science Foundation of China, grant number 51975049.

Informed Consent Statement: Informed consent was obtained from all subjects involved in the study.

Data Availability Statement: All data included in this study are available upon request by contacting with the corresponding author.

Conflicts of Interest: The authors declare no conflict of interest.

References

1. Gao, P.; Zhang, G.; Lv, X. Model-Free Hybrid Control with Intelligent Proportional Integral and Super-Twisting Sliding Mode Control of PMSM Drives. *Electronics* **2020**, *9*, 1427. [CrossRef]
2. Xing, J.; Qin, Z.; Lin, C.; Jiang, X. Research on Startup Process for Sensorless Control of PMSMs Based on I-F Method Combined with an Adaptive Compensator. *IEEE Access* **2020**, *8*, 70812–70821. [CrossRef]
3. Inoue, Y.; Kawaguchi, Y.; Morimoto, S.; Sanada, M. Performance Improvement of Sensorless IPMSM Drives in a Low-Speed Region Using Online Parameter Identification. *IEEE Trans. Ind. Appl.* **2011**, *47*, 798–804. [CrossRef]
4. Verrelli, C.M.; Bifaretti, S.; Carfagna, E.; Lidozzi, A.; Solero, L.; Crescimbini, F.; Di Benedetto, M. Speed Sensor Fault Tolerant PMSM Machines: From Position-Sensorless to Sensorless Control. *IEEE Trans. Ind. Appl.* **2019**, *55*, 3946–3954. [CrossRef]
5. Wang, Q.; Wang, S.; Chen, C. Review of sensorless control techniques for PMSM drives. *IEEJ Tran.* **2019**, *14*, 1543–1552. [CrossRef]
6. Du, B.; Han, S.; Cui, S. Application of Linear Active Disturbance Rejection Controller for Sensorless Control of Internal Permanent-magnet Synchronous Motor. *IEEE Trans. Ind. Appl.* **2016**, *63*, 3019–3027. [CrossRef]
7. Zhang, G. Pseudorandom-Frequency Sinusoidal Injection for Position Sensorless IPMSM Drives Considering Sample and Hold Effect. *IEEE Trans. Power Electron.* **2019**, *34*, 9929–9941. [CrossRef]
8. Yoon, Y.; Sul, S.; Morimoto, S.; Ide, K. High-Bandwidth Sensorless Algorithm for AC Machines Based on Square-Wave-Type Voltage Injection. *IEEE Trans. Ind. Appl.* **2011**, *47*, 1361–1370. [CrossRef]
9. Wang, G.; Valla, M.; Solsona, J. Position Sensorless Permanent Magnet Synchronous Machine Drives-A Review. *IEEE Trans. Ind. Electron.* **2020**, *67*, 5830–5842. [CrossRef]
10. Qiao, Z.; Shi, T.; Wang, Y.; Yan, Y.; Xia, C.; He, X. New Sliding-Mode Observer for Position Sensorless Control of Permanent-Magnet Synchronous Motor. *IEEE Trans. Ind. Electron.* **2013**, *60*, 710–719. [CrossRef]
11. Michalski, T.; Lopez, C.; Garcia, A.; Romeral, L. Sensorless Control of Five Phase PMSM Based on Extended Kalman Filter. In Proceedings of the 42nd Annual Conference of the IEEE-Industrial-Electronics-Society, Florence, Italy, 24–27 October 2016.
12. Kim, H.; Son, J.; Lee, J. A High-Speed Sliding-Mode Observer for the Sensorless Speed Control of a PMSM. *IEEE Trans. Ind. Electron.* **2011**, *58*, 4069–4077. [CrossRef]
13. Zhao, W.; Jiao, S.; Chen, Q.; Xu, D.; Ji, J. Sensorless Control of a Linear Permanent-Magnet Motor Based on an Improved Disturbance Observer. *IEEE Trans. Ind. Electron.* **2018**, *65*, 9291–9300. [CrossRef]
14. Boldea, I.; Paicu, M.C.; Andreescu, G.D. Active flux concept for motion-sensorless unified AC drives. *IEEE Trans. Power Electron.* **2008**, *23*, 2612–2618. [CrossRef]
15. Gong, L.; Zhu, Z. Robust Initial Rotor Position Estimation of Permanent Magnet Brushless AC Machines with Carrier-Signal-Injection-Based Sensorless Control. *IEEE Trans. Ind. Appl.* **2013**, *49*, 2602–2609. [CrossRef]
16. Wu, C.; Zhao, Y.; Sun, M. Enhancing Low-Speed Sensorless Control of PMSM Using Phase Voltage Measurements and Online Multiple Parameter Identification. *IEEE Trans. Power Electron.* **2020**, *35*, 10700–10710. [CrossRef]
17. Boldea, I.; Paicu, M.C.; Andreescu, G.D.; Blaabjerg, F. DTFC-SVM sensorless control of IPMSM. *IEEE Trans. Energy Convers.* **2009**, *24*, 314–322. [CrossRef]
18. Paicu, M.C.; Boldea, I.; Andreescu, G.D.; Blaabjerg, F. Very low speed performance of active flux based sensorless control: Interior permanent magnet synchronous motor vector control versus direct torque and flux control. *IET Electr. Power Appl.* **2009**, *3*, 551–561. [CrossRef]
19. Wang, Y.; Xu, Y.; Zou, J. Sliding-mode sensorless control of PMSM with inverter nonlinearity compensation. *IEEE Trans. Power Electron.* **2019**, *34*, 10206–10220. [CrossRef]
20. Mario, A.H.; Jonatan, R.F.; Alejandro, G.; Marcos, G.J.; Daniel, O.C. Adaptive dead-time compensation for grid-connected PWM inverters of single-stage PV systems. *IEEE Trans. Power Electron.* **2013**, *28*, 2816–2825. [CrossRef]
21. Fausto, S.; Arzhang, Y.T.; Shafiq, O.; Gianmario, P.; Pericle, Z. An accurate self-commissioning technique for matrix converters applied to sensorless control of synchronous reluctance motor drives. *IEEE J. Emerg. Sel. Top. Power Electron.* **2019**, *7*, 1342–1351. [CrossRef]
22. Silverio, B.; Lucas, P.; Mauro, Z. Repetitive-control-based self-commissioning procedure for inverter nonidealities compensation. *IEEE Trans. Ind. Appl.* **2008**, *44*, 1587–1596. [CrossRef]
23. Gianmario, P.; Paolo, G.; Eric, A.; Radu, I.B. Self-commissioning algorithm for inverter nonlinearity compensation in sensorless induction motor drives. *IEEE Trans. Ind. Appl.* **2010**, *46*, 1416–1424. [CrossRef]
24. Nicola, M.; Nicola, C. Sensorless Fractional Order Control of PMSM Based on Synergetic and Sliding Mode Controllers. *Electronics* **2020**, *9*, 1494. [CrossRef]
25. Wang, Z.; Lu, K.; Blaabjerg, F. A Simple Startup Strategy Based on Current Regulation for Back-EMF-Based Sensorless Control of PMSM. *IEEE Trans. Power Electron.* **2012**, *27*, 3817–3825. [CrossRef]
26. Chen, J.; Wu, X.; Chen, S.; Tan, G. Sensorless flux adaption DTFC of an IPMSM based on an active flux-based MTPA and an adaptive second-order sliding mode observer. *IET Power Electron.* **2020**, *13*, 1875–1884. [CrossRef]
27. Foo, G.; Rahman, M.F. Sensorless Direct Torque and Flux-Controlled IPM Synchronous Motor Drive at Very Low Speed Without Signal Injection. *IEEE Trans. Ind. Electron.* **2010**, *57*, 395–403. [CrossRef]
28. Ancuti, M.C.; Tutelea, L.; Andreescu, G.D.; Blaabjerg, F.; Lasucus, C.; Boldea, I. Practical Wide-speed-range Sensorless Control System for Permanent Magnet Reluctance Synchronous Motor Drives via Active Flux Model. *Electr. Power Compon. Syst.* **2014**, *42*, 91–102. [CrossRef]

29. Park, C.S.; Jung, T.U. Online Dead Time Effect Compensation Algorithm of PWM Inverter for Motor Drive Using PR Controller. *J. Electr. Eng. Technol.* **2017**, *12*, 1137–1145. [CrossRef]
30. TMS320F2803x Microcontrollers, Texas Instruments, Dallas, Literature Number SPRS584N. June 2020. Available online: https://www.ti.com/product/TMS320F28035?keyMatch=2803X&tisearch=Search-EN-everything&usecase=GPN#tech-docs. (accessed on 19 January 2021).